Supporting Information

Rodrigues et al. 10.1073/pnas.1609604113

SI Materials and Methods

General Methods. All *B. subtilis* strains were derived from the prototrophic strain PY79 (26). Sporulation was induced by resuspension at 37 °C according to the method of Sterlini-Mandelstam (28) or by exhaustion in supplemented Difco Sporulation medium [8 g/L bacto nutrient broth (Difco), 0.1% (wt/vol) KCl, 1 mM MgSO4, 0.5 mM NaOH, 1 mM Ca(NO3)2, 0.01 mM MnCl2, 0.001 mM FeSO4] (29). Sporulation efficiency was determined in 24- to 30-h cultures as the total number of heat-resistant (80 °C for 20 min) cfus compared with wild-type heat-resistant cfus. Deletion mutants were generated by isothermal assembly and direct transformation into *B. subtilis*.

Fluorescence Microscopy. Fluorescence microscopy was performed with an Olympus BX61 microscope as previously described (7). Cells were mounted on a 2% agarose pad containing resuspension medium using a gene frame (Bio-Rad). Fluorescent signals were visualized with a phase-contrast objective (UplanF1 100×) and were captured with a monochrome CoolSNAPHQ digital camera (Photometrics) using MetaMorph software version 6.1 (Universal Imaging). The membrane dye 1-(4-(trimethylamino)phenyl)-6-phenylhexa-1,3,5-triene (TMA-DPH) (Molecular Probes) was used at a final concentration of 0.01 mM; exposure times typically were 200 ms. Images were analyzed, adjusted, and cropped using MetaMorph software.

Immunoblot Analysis. Whole-cell lysates from sporulating cells (induced by resuspension) were prepared as described previously (7). Samples were heated for 10 min at 50 °C before loading. Equivalent loading was based on OD_{600} at the time of harvest. Proteins were separated by SDS/PAGE on 12.5% polyacrylamide gels, electroblotted onto Immobilon-P membranes (Millipore), and blocked in 5% (wt/vol) nonfat milk in PBS and 0.5% Tween-20. The blocked membranes were probed with anti-SpoIID (1:10,000), anti-SpoIIIAH (1:10,000), anti-SigA (1:10,000), anti-EzrA (1:10,000), and anti-SpoIIIAG (1:10,000), diluted into 3% (wt/vol) BSA in 1× PBS-0.05% Tween-20. Primary antibodies were detected using HRP-conjugated goat, anti-rabbit IgG (1:20,000, Bio-Rad) and the Western Lightning reagent kit as described by the manufacturer (PerkinElmer).

Protease Susceptibility. Protease susceptibility assays were performed in sporulating cells lacking the SpoIIQ (Q) protein (strain BCR267) to ensure that the membrane proteins present in the inner and outer forespore membranes would not be artificially inaccessible because of protoplast engulfment (30). Twenty-five milliliters of sporulating cells (induced by resuspension) were harvested by centrifugation at hour 2 after the onset of sporulation, washed, and resuspended in 2 mL 1× SMM buffer (0.5 M sucrose, 20 mM $MgCl_2$, 20 mM maleic acid, pH 6.5). The cells were protoplasted by lysozyme (5 mg/mL final concentration) for 10 min with slow agitation. The protoplasts were harvested by centrifugation and resuspended in 1 mL of 1× SMM. Protoplasts (100 μL) were incubated with trypsin (30 μg/mL final concentration) (Worthington), trypsin and Triton X-100 (2% final concentration), or 1× SMM for 15 min. Reactions were terminated by the addition of 100 μL of 2× SDS-sample buffer and incubation for 5 min at 95 °C. Five microliters from each reaction were analyzed by immunoblot.

Protein Expression and Purification. All recombinant proteins were overexpressed in *E. coli* Rosetta (DE3) pLysS and purified with a 6×His-SUMO (H-SUMO) tag fused to their N termini (27). Cells were grown in 2 L of Terrific Broth (TB) medium [1.2% (wt/vol) tryptone, 2.4% (wt/vol) yeast extract, 0.4% (vol/vol) glycerol, 0.017 M potassium phosphate dibasic, 0.072 M potassium phosphate monobasic] supplemented with ampicillin (50 μg/mL) at 37 °C to an OD_{600} of 0.8 and induced by the addition of isopropyl β-D-1-thiogalactopyranoside (IPTG) to 0.5 mM after the cultures were cooled to 25 °C. Growth was continued overnight at 25 °C, and cells were harvested by centrifugation. Cell pellets were resuspended in 1/25th volume of buffer A [50 mM Tris·HCl (pH 8.0), 500 mM NaCl, 10% (vol/vol) glycerol] containing 25 mM imidazole and the Complete mixture of protease inhibitor (Roche). Cells were lysed by six passages through a Microfluidizer M110-P (Microfluidics) at 10,000 psi, and cell debris was pelleted by centrifugation at 40,000 × *g* for 30 min at 4 °C. H-SUMO fusions were purified using 8.0 mL Ni-NTA agarose resin (Qiagen) equilibrated in buffer A with 25 mM imidazole. After loading and extensive washing with buffer A containing 50 mM imidazole, the fusion proteins were eluted with a linear 50–500 mM gradient of imidazole in buffer B [50 mM Tris·HCl (pH 8.0), 300 mM NaCl, 10% (vol/vol) glycerol] over 10 column volumes. Peak fractions were pooled and dialyzed overnight at 4 °C in buffer B containing 25 mM imidazole and a 1:500 dilution of a 6×His-tagged Ulp (SUMO) protease (H-SP) preparation (27). Cleavage reactions were passed through Ni-NTA resin to remove free H-SUMO and H-SP, and untagged proteins were collected in the flow through. Flow-through fractions were concentrated with Amicon Ultra Centrifugal filter units with a molecular weight cutoff of 10,000 (Millipore) and were injected onto a 10/300 GL Superdex 200 gel-filtration column (GE Healthcare). Proteins were eluted with buffer C [25 mM Tris·HCl (pH 8.0), 150 mM NaCl] and again concentrated with Amicon Ultra Centrifugal filter units. Protein standards used for calibration were ovalbumin (44 kDa), conalbumin (75 kDa), aldolase (158 kDa), and thyroglobulin (669 kDa) (GE Healthcare). Blue Dextran 2000 (GE Healthcare) was used to determine the void volume of the gel-filtration column. Protein concentrations were measured using absorbance at 280 nm.

Analytical Ultracentrifugation Analysis. Sedimentation velocity experiments were carried out on an analytical ultracentrifuge XLI (Beckman Coulter) with a rotor speed of 130,000 × *g*, at 20 °C, using an Anti-50 rotor and double-sector cells with an optical path length of 12 or 3 mm equipped with sapphire windows. Acquisitions were made using absorbance at 280 nm. Two samples of AG_{Bsu} D1+D2 (0.6 and 3 mg/mL) in buffer C were investigated. Solvent density of 1.004 g/mL and viscosity of 1.054 mPa/s were measured at 20 °C on a DMA 5000 density meter and an AMVn viscosity meter (Anton Paar), respectively, and the partial specific volume was estimated to 0.734 mL/g with the program SEDNTERP. The analysis was carried out in terms of distribution of sedimentation coefficients [$c(s)$] and noninteracting species with SEDFIT software, version 14.1.

EM. Samples of AG_{Bsu} D1+D2 were diluted to 0.1 mg/mL in buffer C. For negative-stain EM analysis, 3 μL of the sample was loaded on the clean side of carbon on mica (carbon/mica interface), negatively stained with 2% (wt/vol) sodium silico tungstate, and air-dried. Images were collected on a Tecnai 12 microscope (FEI) with a LaB_6 electron source operating at 120 kV and equipped with a GATAN camera (Orius 1000). For cryo-EM analysis, 3 μL of the AG_{Bsu} D1+D2 sample at 0.4 mg/mL was loaded onto a Quantifoil R2/1 holey grid (Quantifoil Micro Tools GmbH) and then vitrified using a Mark IV Vitrobot (FEI). The frozen grids were transferred onto a Polara electron microscope working at 300 kV. The images were taken under

low-dose conditions (<20 e/Å^2) with a nominal magnification of 59,000×, recorded on Kodak SO-163 films, and developed for 12 min in full-strength Kodak D19 developer. Negatives were digitized on a PhotoScan TD scanner (Z/I Imaging) at a step size of 7 μm, corresponding to 1.19 Å per pixel. The images were corrected for the Contrast Transfer Function using CTFFIND3 (31). Then 6,125 particles were selected semiautomatically from 30 films using the EMAN boxer routine (32); these particles were normalized and filtered between 200 Å and 20 Å (Fig. S2 *C* and *D*). SPIDER (33) was used for projection-matching image analysis. The initial model was generated by back-projecting a side view and imposing C24 symmetry (as determined by ultracentrifugation experiments). Several models were generated and averaged to give a 50-Å initial model. The angular step used in the projection-matching procedure was 5°, giving 20 equally spaced reprojections. A lack of side views limited the final resolution to 35 Å as indicated by the standard Fourier-shell correlation (criterion FSC = 0.5) (34). Ab initio classification of the particle images using RELION (35) generated classes that were coherent with the 3D model obtained using SPIDER (Fig. 2*E*).

3D Homology Modeling of the AG_{Bsu} Monomer. Homology modeling servers, including Phyre2 (www.sbg.bio.ic.ac.uk/phyre2/), Robetta (www.robetta.org/), and Swiss Model (https://swissmodel.expasy.org/) (22), were tested to generate models of AG_{Bsu}. All identified EscJ [Protein Databank (PDB) ID code 1YJ7] and PrgK (PDB ID code 3J6D) as the best templates to model the D2 domain of AG_{Bsu}. Using the Swiss Model server, we used the structures of EscJ (PDB ID code 1YJ7) and PrgK (PDB ID code 3J6D) separately as target-template alignment files. Both AG_{Bsu} D2 models had high-confidence factors in the regions homologous to the EscJ/PrgK family. The model based on EscJ displayed a global QMEAN scoring function of −3.52 and a sequence identity with AG_{Bsu} D2 of 24% over 85 residues. The model based on PrgK had a global QMEAN scoring function of −10.44 and a sequence identity of 17% over 85 residues. The insertion region was modeled with lower-confidence values. When analyzed with servers dedicated to secondary structure predictions (PSIPRED, bioinf.cs.ucl.ac.uk/psipred/; JPRED, www.compbio.dundee.ac.uk/jpred/; and PredictProtein, https://www.predictprotein.org/), this region was predicted to be composed mainly of β secondary elements. Because the Swiss model based on EscJ contained only helices and loops in the insertion region, whereas the model based on PrgK contained a large antiparallel β-hairpin that matches the PSIPRED, JPRED, and PredictProtein predictions, we used the Swiss model based on PrgK (Fig. S3) for modeling the AG_{Bsu} ring.

EM-Guided Symmetry Modeling of the AG_{Bsu} Ring. To model the ring, we only used the regions of the AG_{Bsu} monomer that could be modeled with a confidence factor >0.2 and displayed secondary structures in agreement with PSIPRED, JPRED, and PredictProtein predictions. We split the model of the D2 monomer into two PDB files, one corresponding to the regions homologous to the EscJ/PrgK family (residues 90–123 and 181–224), and the other corresponding to the insertion region (residues 129–154). Each PDB file was placed manually and independently into the EM map density according to its putative localization. Then 24-fold symmetry files were generated using a "pdbsymm" symmetry builder script from the Situs 2.7 package (36). Finally, the position of the protomers in the EM map were refined using the "Fit in map" function in Chimera (37) and were energy minimized using the NAMD program (23).

Protein–Protein Interaction Assay. Samples of AG_{Bsu} rings at 5 mg/mL in buffer C were incubated for 15 min at room temperature with stoichiometric amounts of the purified extracellular domains of *B. subtilis* AH, Q, or preformed AH/Q complexes. After incubation, samples were injected onto a 10/300 GL Superdex 200 gel-filtration column (GE Healthcare) and eluted with buffer C. In all cases, the elution volume of the oligomeric species was indistinguishable from the elution volume of the AG_{Bsu} rings alone (~8.5 mL), providing no evidence of a higher-order complex. However, the oligomeric species were analyzed by negative-stain EM using the protocol described above. The EM images revealed ring-shaped structures with architecture and dimensions similar to those of AG_{Bsu} rings alone, further indicating that, under these experimental conditions, higher-order complexes between AG, AH, and/or Q do not exist.

Plasmid Construction.

pCR094 [*His6-SUMO-spoIIIAG* (51-229, *B. subtilis*)] was generated by isothermal assembly of a PCR product containing the relevant DNA segment of *spoIIIAG* (oligonucleotide primers oCR160 and oCR161 on PY79 genomic DNA) into pTB146 (His6-SUMO) cut with SapI. pTB146 (His6-SUMO) is a protein expression vector provided by T. Bernhardt, Harvard Medical School.

pCR133 [*His6-SUMO-spoIIIAG* (90-229, *B. subtilis*)] was generated by isothermal assembly of a PCR product containing the relevant DNA segment of *spoIIIAG* (oligonucleotide primers oCR161 and oCR302 on PY79 genomic DNA) into pTB146 (His6-SUMO) cut with SapI. pTB146 (His6-SUMO) is a protein expression vector provided by T. Bernhardt, Harvard Medical School.

pCR134 [*His6-SUMO-spoIIIAG* (66-201, *A. longum*)] was generated by a two-way ligation of a BamHI-XhoI gBlock (IDT Technologies) containing the relevant DNA segment of $spoIIIAG_{Alo}$ (NCBI protein accession number WP_004095879.1) into pTB146 (His6-SUMO) cut with BamHI-XhoI.

pCR137 [*His6-SUMO-spoIIIAG* (78-212, *G. thermodenitrificans*)] was generated by a two-way ligation of a BamHI-XhoI gBlock (IDT Technologies) containing the relevant DNA segment of $spoIIIAG_{Gth}$ (accession number WP_008879812.1) into pTB146 (His6-SUMO) cut with BamHI-XhoI.

pCR244 [*His6-SUMO-spoIIIAG*^{R209E} (51-229, *B. subtilis*)] was generated by site-directed mutagenesis using oligonucleotide primers oCR515 and oCR516 and pCR094.

pCR245 [*His6-SUMO-spoIIIAG*^{K223E} (51-229, *B. subtilis*)] was generated by site-directed mutagenesis using oligonucleotide primers oCR517 and oCR518 and pCR094.

pCR247 [*His6-SUMO-spoIIIAG*^{R209A} (51-229, *B. subtilis*)] was generated by site-directed mutagenesis using oligonucleotide primers oCR521 and oCR522 and pCR094.

pCR248 [*His6-SUMO-spoIIIAG*^{K223A} (51-229, *B. subtilis*)] was generated by site-directed mutagenesis using oligonucleotide primers oCR523 and oCR524 and pCR094.

pCR257 [*yhdG::PspoIIIA (2)-spoIIIAG (kan)*] was generated by a two-way ligation of a BamHI-XhoI PCR product (oligonucleotide primers oCR486 and oCR433 on PY79 genomic DNA) containing the relevant DNA segment of into pBB283 (yhdG::kan) cut with BamHI-XhoI. pBB283 (yhdG::kan) is a double-crossover ectopic integration vector provided by B. Burton and D. Z. Rudner, Harvard Medical School.

pCR258 [*yhdG::PspoIIIA (2)-spoIIIAG*^{R209E} *(kan)*] was generated by site-directed mutagenesis using oligonucleotide primers oCR515 and oCR516 and pCR257.

pCR259 [*yhdG::PspoIIIA (2)-spoIIIAG*^{K223E} *(kan)*] was generated by site-directed mutagenesis using oligonucleotide primers oCR517 and oCR518 and pCR257.

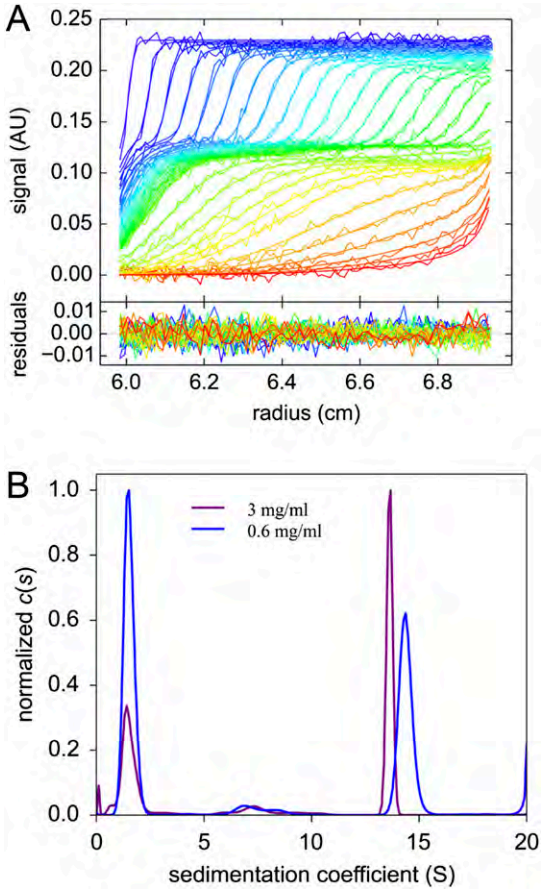

Fig. S1. Biochemical characterization of AG_{Bsu}. (*A*) Analytical ultracentrifugation analysis of AG_{BSu} D1+D2 (at 3 mg/mL). The superposition of experimental and fitted sedimentation velocity profiles (*Upper*) and their differences (*Lower*) are shown. (*B*) Sedimentation coefficient distributions obtained for AG_{BSu} D1+D2 at 3 and 0.6 mg/mL.

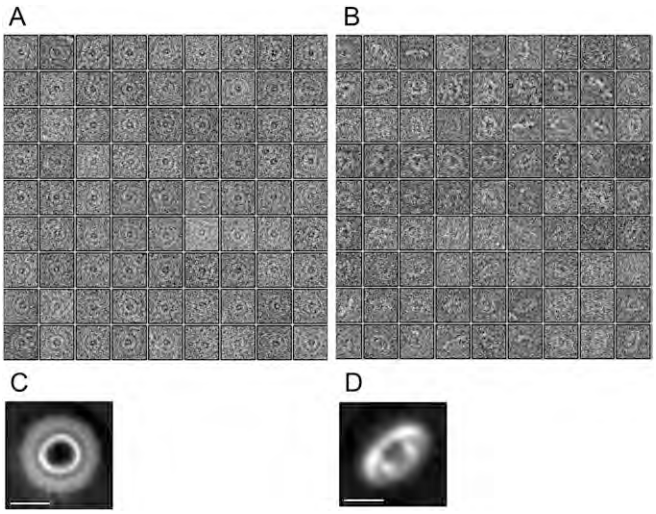

Fig. S2. AG_{Bsu} forms a large oligomeric complex. (*A* and *B*) Selection of 81 cryo-EM images of the AG_{BSu} D1+D2 ring particles seen in top (*A*) or side (*B*) orientations. (*C* and *D*) Class averages of AG_{Bsu} D1+D2 ring particles in top (*C*) and side (*D*) orientations obtained by ab initio classification using RELION. (Scale bars, 10 nm.)

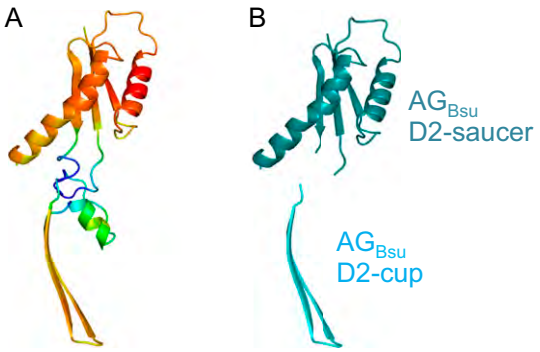

Fig. S3. 3D modeling of the AG_{Bsu} ring. (*A*) Ribbon representation of the raw AG_{Bsu} D2 model colored by model quality value. Red corresponds to regions with high-quality values (~0.8) and are built on X-ray structures. Blue regions have low-quality values (~0.1) and are built from loop databases without template contribution. (*B*) Ribbon representation of the domains in the AG_{Bsu} D2 model that were used for modeling the AG_{Bsu} D2 ring in the cup (AG_{Bsu} D2-cup, in cyan) and saucer (AG_{Bsu} D2-saucer, in teal).

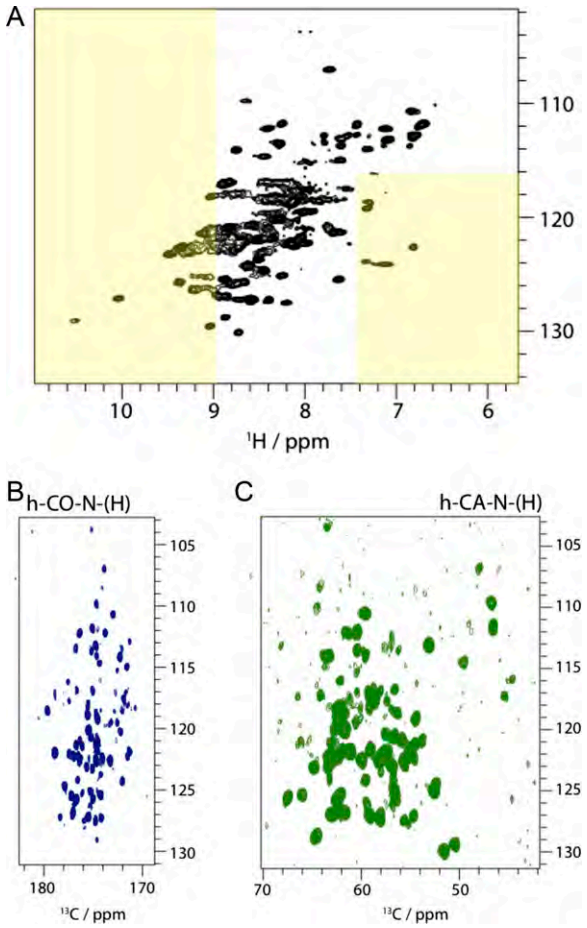

Fig. S4. Solid-state NMR studies of AG_{Bsu} D1+D2. NMR spectra obtained on AG_{Bsu} D1+D2 (~1.5 mg), using proton-detected solid-state magic-angle-spinning (MAS) NMR, obtained at 55-kHz MAS frequency at a magnetic field strength of 14.1 T at an effective sample temperature of 22 ± 2 °C. (*A*) 2D H–N correlation spectrum. Narrow peak widths indicate a high degree of sample homogeneity and symmetry among the rings. The dispersion of amide signals, over more than 3 ppm in the ^{1}H dimension strongly suggests that the rings contain β-strand structures. Yellow rectangles show the region of the spectrum where β-sheet signals are typically found. Amide signals in β-sheets do not necessarily lie in these regions, but signals in these regions are most often caused by β-sheets. The two signals shifted down-field at >10 ppm are backbone amide signals, and their strong down-field shift strongly suggests that these residues have a β-sheet conformation of these residues. AG_{Bsu} D1+D2 does not contain Trp residues, excluding the possibility that these signals arise from Trp side chains. (*B* and *C*) 3D CO-N-H (*B*) and CA-N-H (*C*) correlation experiments. Both experiments are 2D projections along the ^{1}H dimension. Experiments were performed with cross-polarization schemes, which focus exclusively on rigid proteins, i.e., all the observed signals arise from residues in rigid structures. Taken together, the solid-state NMR data suggest that AG_{Bsu} D1+D2 rings form rigid structures containing a high proportion of β-sheet conformations.

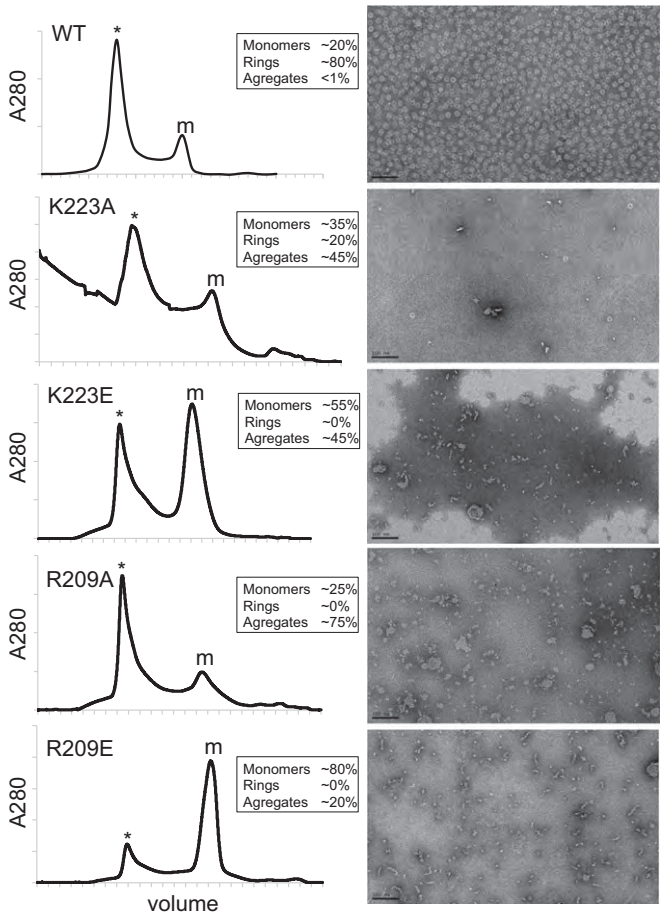

Fig. S5. In vitro test of the AG ring model. Size-exclusion chromatography of purified wild-type AG_{Bsu} D1+D2 and the indicated mutants. (*Left*) Elution volumes from a Superdex 200 column are plotted on the *x* axis, and the 280-nm absorbance is plotted on the *y* axis. The elution peaks containing AG_{Bsu} D1+D2 monomers (m) and rings and/or aggregates (*) are indicated. (*Right*) Negative-stain EM images of the aggregate/oligomer fractions. (Scale bars, 100 nm.) The percentage of monomers, rings, and aggregates based on size exclusion and EM is indicated for each purified protein.

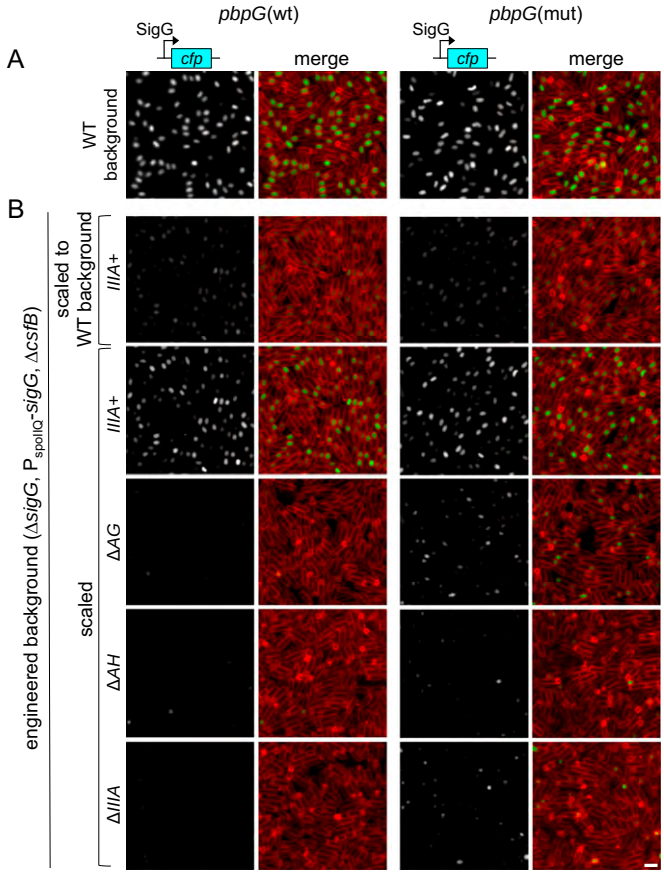

Fig. S6. Partial bypass of the *spoIIIA* operon in sporulating cells with a mutation in *pbpG*. (*A*) SigG activity (assessed using P_{sspB}-*cfp*) in wild-type sporulating cells harboring wild-type *pbpG* (*Left*) or a *pbpG* mutant (*pbpG ΔR147-K1480*) (*Right*). Images are from hour 4 of sporulation. Images are P_{sspB}-CFP (*Left*) and merged with TMA-DPH membrane staining (*Right*). These strains are shown for comparison with the strains in *B*. (*B*) SigG activity (P_{sspB}-*cfp*) in sporulating cells engineered to bypass SigG autoregulation and lacking the SigG inhibitor CsfB (Gin). Strains harbor the wild-type *spoIIIA* operon (*IIIA*+) or lack AG (Δ*AG*), AH (Δ*AH*), or the entire operon (Δ*IIIA*) and contain the wild-type *pbpG* gene (*Left*) or a *pbpG* mutant (*pbpG ΔR147-K148*) (*Right*). The first row of panels in *B* was scaled identically to the panels in *A*. The remaining panels in *B* were scaled relative to each other. Strains engineered to bypass autoregulation and lacking CsfB have reduced SigG activity compared with the wild-type strain. The *pbpG* mutation partially bypasses the requirement of AG or the entire *spoIIIA* operon (including AH) for SigG activity. The nature of the weaker bypass in the absence of AH in this background is currently unknown. (Scale bar, 2 μm.)

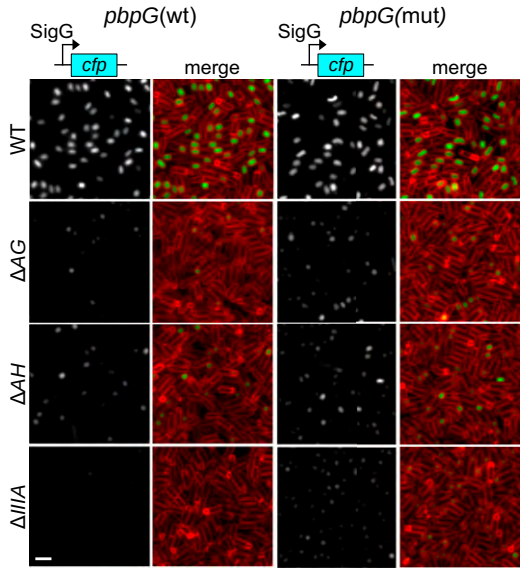

Fig. S7. A *pbpG* mutation partially bypasses the requirement for the *spoIIIA* operon. Analysis of SigG activity in sporulating cells harboring the indicated mutants in the A–Q complex in the presence of wild-type *pbpG* (*Left*) or a *pbpG* mutant (*pbpG ΔR147-K148*) (*Right*). For cells containing wild-type *pbpG*, the strains used were wild-type (BCR877), Δ*AG* (BCR878), Δ*AH* (BCR879), and Δspo*IIIA* (*ΔIIIA*) operon-null (BCR990). For the mutant *pbpG* (mut) allele, the strains used were wild-type (BCR896), Δ*AG* (BCR959), Δ*AH* (BCR900), and Δ*IIIA* (BCR991). Images are P_{sspB}-CFP (*Left*) and merged with TMA-DPH–stained membranes (*Right*). The images were scaled identically. (Scale bar, 2 μm.)

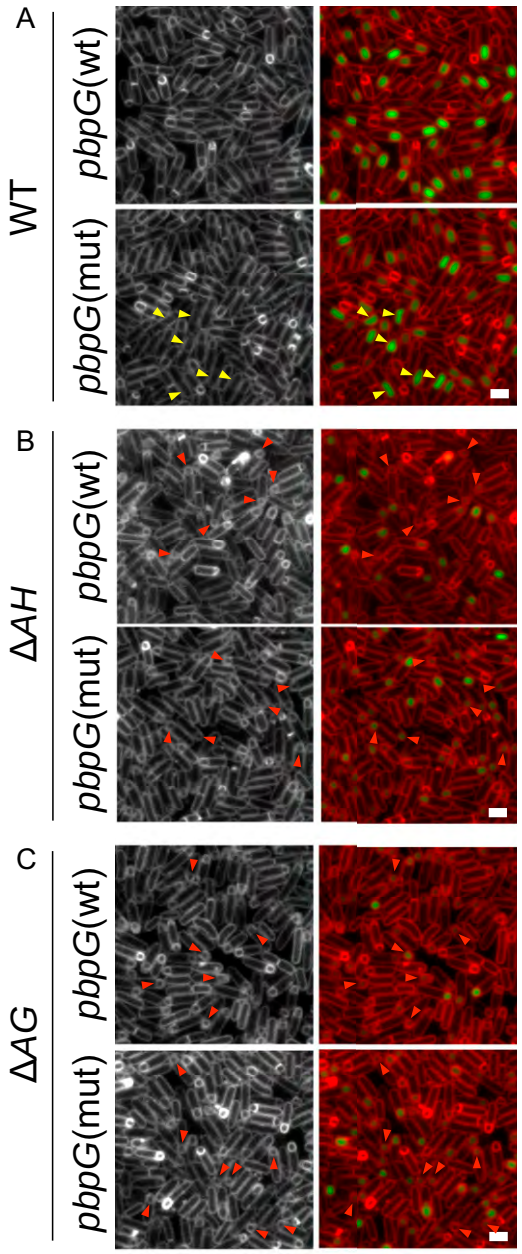

Fig. S8. The *pbpG* mutation does not suppress the forespore morphology defects of the Δ*AH* and Δ*AG* mutants. Representative images of SigG activity and forespore morphology assessed with the membrane dye TMA-DPH in strains harboring wild-type *pbpG* or a *pbpG* mutant (*pbpG ΔR147-K148*) in wild-type cells (*A*), in cells lacking AH (Δ*AH*) (*B*), and in cells lacking AG (Δ*AG*) (*C*). Images are from hour 4 of sporulation. We note that sporulating cells harboring the *pbpG* mutation exhibit forespore morphology defects that are different from the small and collapsed forespores observed in cells lacking members of the A–Q complex. Yellow arrowheads point to forespores with abnormal morphologies in the *pbpG* mutant, and red arrowheads point to forespores that failed to thrive and/or collapsed. Images show TMA-DPH–stained membrane (*Left*) and merged with P_{sspB}-CFP (*Right*). (Scale bars, 2 μm.)

Table S1. Strains, plasmids, and oligonucleotides

Construct	Genotype/description/sequence	Source or reference
B. subtilis strains		
PY79	Prototrophic wild type	(26)
BCR267	*spoIIQ::kan*	This work
BCR776	*spoIIIAG::markerless*	
BCR859 (AHB1331)	*spoIIIGΔ1, amyE::PspoIIQ-sigG::spec, ΔcsfB::tet, ywrK::Tn917::amyE::PsspB-cfp(Bs)::cat*	(4)
BCR877	*ywrK::Tn917::amyE::PsspB-cfp(Bs)::cat*	This work
BCR878	*spoIIIAG::markerless, ywrK::Tn917::amyE::PsspB-cfp(Bs)::cat*	This work
BCR879	*spoIIIAH::erm, ywrK::Tn917::amyE::PsspB-cfp(Bs)::cat*	This work
BCR896	*ywrK::Tn917::amyE::PsspB-cfp(Bs)::cat, pbpG(ΔR147-K148)Ωphleo*	This work
BCR900	*spoIIIAH::erm, ywrK::Tn917::amyE::PsspB-cfp(Bs)::cat, pbpG(ΔR147-K148)Ωphleo*	This work
BCR929	*spoIIIGΔ1, amyE::PspoIIQ-sigG::spec, ΔcsfB::tet, ywrK::Tn917::amyE::PsspB-cfp(Bs)::cat, spoIIIAH::erm*	This work
BCR935	*spoIIIGΔ1, amyE::PspoIIQ-sigG::spec, ΔcsfB::tet, ywrK::Tn917::amyE::PsspB-cfp(Bs)::cat, spoIIIA::kan*	This work
BCR946	*spoIIIGΔ1, amyE::PspoIIQ-sigG::spec, ΔcsfB::tet, ywrK::Tn917::amyE::PsspB-cfp(Bs)::cat, spoIIIAG::markerless*	This work
BCR959	*spoIIIAG::markerless, ywrK::Tn917::amyE::PsspB-cfp(Bs)::cat, pbpG(ΔR147-K148)Ωphleo*	This work
BCR961	*spoIIIGΔ1, amyE::PspoIIQ-sigG::spec, ΔcsfB::tet, ywrK::Tn917::amyE::PsspB-cfp(Bs)::cat, spoIIIAH::erm, pbpG(ΔR147-K148)Ωphleo*	This work
BCR964	*spoIIIGΔ1, amyE::PspoIIQ-sigG::spec, ΔcsfB::tet, ywrK::Tn917::amyE::PsspB-cfp(Bs)::cat, spoIIIA::kan, pbpG(ΔR147-K148)Ωphleo*	This work
BCR976	*spoIIIGΔ1, amyE::PspoIIQ-sigG::spec, ΔcsfB::tet, ywrK::Tn917::amyE::PsspB-cfp(Bs)::cat, spoIIIAG::markerless, pbpG(ΔR147-K148)Ωphleo*	This work
BCR990	*ywrK::Tn917::amyE::PsspB-cfp(Bs)::cat, spoIIIA::kan*	This work
BCR991	*ywrK::Tn917::amyE::PsspB-cfp(Bs)::cat, pbpG(ΔR147-K148)Ωphleo, spoIIIA::kan*	This work
BCR992	*spoIIIGΔ1, amyE::PspoIIQ-sigG::spec, ΔcsfB::tet, ywrK::Tn917::amyE::PsspB-cfp(Bs)::cat, pbpG(ΔR147-K148)Ωphleo*	This work
BCR1434	*spoIIIAG::markerless, yhdG::PspoIIIA (2)-spoIIIAG (kan)*	This work
BCR1435	*spoIIIAG::markerless, yhdG::PspoIIIA (2)-spoIIIAG^{R209E} (kan)*	This work
BCR1436	*spoIIIAG::markerless, yhdG::PspoIIIA (2)-spoIIIAG^{K223E} (kan)*	This work
BCR1437	*spoIIIAG::markerless, ycgO::PsspB-RBSopt-gfp (spec)*	This work
BCR1438	*spoIIIAG::markerless, yhdG::PspoIIIA (2)-spoIIIAG (kan), ycgO::PsspB-RBSopt-gfp (spec)*	This work
BCR1439	*spoIIIAG::markerless, yhdG::PspoIIIA (2)-spoIIIAG^{R209E} (kan), ycgO::PsspB-RBSopt-gfp (spec)*	This work
BCR1440	*spoIIIAG::markerless, yhdG::PspoIIIA (2)-spoIIIAG^{K223E} (kan), ycgO::PsspB-RBSopt-gfp (spec)*	This work
Plasmids		
pCR094	*His6-SUMO-spoIIIAG* (51-229, *B. subtilis*)	This work
pCR133	*His6-SUMO-spoIIIAG* (90-229, *B. subtilis*)	This work
pCR134	*His6-SUMO-spoIIIAG* (66-201, *A. longum*)	This work
pCR137	*His6-SUMO-spoIIIAG* (78-212, *G. thermodenitrificans*)	This work
pCR244	*His6-SUMO-spoIIIAG^{R209E}* (51-229, *B. subtilis*)	This work
pCR245	*His6-SUMO-spoIIIAG^{K223E}* (51-229, *B. subtilis*)	This work
pCR247	*His6-SUMO-spoIIIAG^{R209A}* (51-229, *B. subtilis*)	This work
pCR248	*His6-SUMO-spoIIIAG^{K223A}* (51-229, *B. subtilis*)	This work
pCR257	*yhdG::PspoIIIA (2)-spoIIIAG (kan)*	This work
pCR258	*yhdG::PspoIIIA (2)-spoIIIAG ^{R209E} (kan)*	This work
pCR259	*yhdG::PspoIIIA (2)-spoIIIAG^{K223E} (kan)*	This work
Oligonucleotides		
oCR160	gctcacagagaacagattggtggttcttcacctgagaaaactgaaaacg	This work
oCR161	tcgacggagctctgctcttctaccttatgaatcctccttttatttttttag	This work
oCR302	gctcacagagaacagattggtggtgctgactcgatcgatgactatgaa	This work
oCR433	cgcggatccttatgaatcctcctttatttttttag	This work
oCR486	gcgctcgagcttttcaagacagaccccgaagt	This work
oCR515	accattatcgaagcggtgacagaggtcctggatgttccaagccac	This work
oCR516	gtggcttggaacatccaggacctctgtcaccgcttcgataatggt	This work
oCR517	caccgggttgcggttgcccctgaaaaaataaaggaggattca	This work
oCR518	tgaatcctcctttatttttcaggggcaaccgcaacccggtg	This work
oCR521	accattatcgaagcggtgacagcggtcctggatgttccaagccac	This work
oCR522	gtggcttggaacatccaggaccgctgtcaccgcttcgataatggt	This work
oCR523	caccgggttgcggttgcccctgcaaaaataaaggaggattca	This work
oCR524	tgaatcctcctttatttttgcaggggcaaccgcaacccggtg	This work